

# Dynamic Nonlocal Dielectric Metasurfaces: Tuning Collective Lattice Resonances via Substrate–Superstrate Permittivity Contrast

Izzatjon Allayarov, Andrey B. Evlyukhin,\* Diane J. Roth, Boris Chichkov, Anatoly V. Zayats,\* and Antonio Calà Lesina\*

Contrary to local resonances of single nanostructures, collective (or nonlocal) resonances in periodic metasurfaces, such as surface lattice resonances (SLRs), can significantly enhance light–matter interaction, leading to higher spectral selectivity. The dynamic control of such nonlocal response represents an emerging field of research. While tuning of SLRs has been demonstrated in plasmonic metasurfaces, the use of dielectric metasurfaces provides additional conditions to control both reflectance and transmittance, with minimum absorption effects. A close-to-homogeneous environment is usually required to guarantee the excitation of SLRs. Here, we propose theoretically and demonstrate experimentally a practical strategy for the tuning of SLRs in dielectric metasurfaces when an arbitrary index mismatch is considered between substrate and superstrate. The approach is based on a generalized lattice sum theory that accounts for the presence of a substrate. Dynamic tuning of the SLRs in silicon metasurfaces placed on a substrate is achieved with a changeable superstrate via an optofluidic process. Two tuning mechanisms are revealed corresponding to shifting and damping of the SLR, depending on the superstrate–substrate refractive index contrast. The demonstrated dynamic manipulation of transmission and reflection may be exploited in dielectric metasurfaces for tunable spectral selectivity, sensing, or novel display technologies.

applications in beam steering, adaptive lenses, augmented reality, optical switches, and displays.<sup>[1,2]</sup> Tunable metasurfaces have been demonstrated using carrier accumulation/depletion via voltage gating,<sup>[3]</sup> liquid crystals,<sup>[4,5]</sup> thermo-optic effect,<sup>[6]</sup> mechanical actuation,<sup>[7]</sup> chemical reactions,<sup>[8]</sup> phase-change materials,<sup>[9,10]</sup> non-linear effects in time-varying materials,<sup>[11]</sup> immersion in low-index and high-index liquids, and with microfluidic channels.<sup>[12–16]</sup> In all these cases, the local response of individual plasmonic or dielectric meta-atoms is primarily affected, influencing the amplitude, phase, or direction of the transmitted and/or reflected light.

Nonlocal metasurfaces are emerging as an alternative approach, where their properties depend on the input field across the entire metasurface or a portion of it.<sup>[17]</sup> Collective (or nonlocal) effects in periodic 2D arrays of nanoparticles, such as collective or surface lattice resonances (SLRs), have been investigated to achieve optical


response typically not obtainable with single particles, such as resonances with high quality factor.<sup>[18]</sup> An SLR occurs if a specific diffraction order of a periodic array becomes an evanescent wave propagating in the plane of the array, the so-called Rayleigh

## 1. Introduction

The ultimate goal of nanophotonic metasurfaces is to achieve a dynamically tunable optical response, required to enable

I. Allayarov, A. Calà Lesina  
Hannover Centre for Optical Technologies  
Leibniz University Hannover  
Nienburger Str. 17, 30167 Hannover, Germany  
E-mail: antonio.calalesina@hot.uni-hannover.de

I. Allayarov, A. Calà Lesina  
Institute of Transport and Automation Technology  
Leibniz University Hannover  
An der Universität 2, 30823 Garbsen, Germany

 The ORCID identification number(s) for the author(s) of this article can be found under <https://doi.org/10.1002/adpr.202300268>.

© 2023 The Authors. Advanced Photonics Research published by Wiley-VCH GmbH. This is an open access article under the terms of the Creative Commons Attribution License, which permits use, distribution and reproduction in any medium, provided the original work is properly cited.

DOI: 10.1002/adpr.202300268

I. Allayarov, A. B. Evlyukhin, B. Chichkov, A. Calà Lesina  
Cluster of Excellence PhoenixD  
Leibniz University Hannover  
Welfengarten 1A, 30167 Hannover, Germany  
E-mail: evlyukhin@iqo.uni-hannover.de

A. B. Evlyukhin, B. Chichkov  
Institute of Quantum Optics  
Leibniz University Hannover  
Welfengarten 1, 30167 Hannover, Germany

D. J. Roth, A. V. Zayats  
Department of Physics and London Centre for Nanotechnology  
King's College London  
Strand, London WC2R 2LS, UK  
E-mail: a.zayats@kcl.ac.uk

anomalies (RAs). The sensitivity of the SLR to the refractive index of the environment and, as a consequence, the modification of the SLR spectral position and its quality factor make this collective effect attractive in sensing applications.<sup>[19–23]</sup>

The SLR concept was initially developed for arrays of metallic nanoparticles with electric dipolar response<sup>[20,24–26]</sup> and later extended to metallic particles supporting high-order plasmonic multipoles.<sup>[27,28]</sup> Design strategies to achieve multiresonant plasmonic metasurfaces based on SLRs were also reported.<sup>[29,30]</sup> Tuneability of SLRs in plasmonic metasurfaces was achieved in the near-infrared regime via postfabrication thermal control<sup>[31]</sup> as well as using electrically controlled liquid crystals.<sup>[32,33]</sup> In the case of SLRs in metallic metasurfaces, as a rule, the focus is on transmission (extinction), because resonant absorption leads to significant suppression of reflection. The concept of the lattice resonances has also been expanded to dielectric metasurfaces supporting Mie resonances.<sup>[34–38]</sup> In the dielectric case, the absorption is significantly lower, which makes it possible to observe resonances also in the reflectance spectra. This allows the development of tunable dielectric metasurfaces based on SLRs for both reflection and transmission.

SLRs can be completely suppressed when the metasurface is in a nonhomogeneous medium due to the destructive contribution of strong reflection from the substrate.<sup>[39,40]</sup> Thus, a close-to-homogeneous environment is generally sought to guarantee the existence of the SLR. This is the case in the above studies on SLR tuneability, where index matching with the glass substrate was achieved using high-index superstrates, such as oil<sup>[31]</sup> and liquid crystals.<sup>[32,33]</sup> Even in the presence of substrate–superstrate mismatch, the simplified approximation of a homogeneous environment is often used to analytically explain the excitation of SLRs.<sup>[31,33]</sup>

In this article, we turn the substrate–superstrate index mismatch into a control parameter to achieve tuneability of the metasurface optical response by modifying the superstrate. We developed a generalized theory for the lattice sum which can account for the substrate–superstrate interface. Contrary to previous works, where the tuneability of SLRs relies on the use of high-index superstrates,<sup>[31–33]</sup> we provide a general design strategy to obtain SLRs in the presence of an arbitrary superstrate, including low-index media such as air.

We show that there are two mechanisms to control the optical response of metasurfaces via SLRs: one providing suppression of the resonance and another resulting in the spectral shift of the resonance. We demonstrate these dynamic tuning principles on the example of a silicon metasurface on a glass substrate and introduce an optofluidic platform using a variable water level as a strategy to control the refractive index of the superstrate. The choice of dielectric metasurfaces is motivated by the fundamentally different physics (based on Mie-type resonance) than their plasmonic counterpart, as well as possible future extensions of the approach to higher-order multipoles. Due to material absorption in silicon, the tuning mechanisms are demonstrated in the red portion of the visible spectrum. However, the approach is general and can be extended to other colors using dielectric materials with lower absorption in the visible.

Both revealed mechanisms provide changes in the optical response of the metasurfaces with the change of the water

environment. The use of water makes the tuning mechanism reversible since water can be totally removed from the metasurface. Liquid environments provide flexibility in using microfluidic control,<sup>[12]</sup> electrowetting effect,<sup>[41]</sup> or simply through thermal evaporation/condensation and can be extended to a variety of liquids beyond water. Furthermore, the switching speed of the metasurface can be regulated by adopting an appropriate microfluidic control technique. Our results demonstrate new practical possibilities for tuning light–matter interaction in nonlocal dielectric metasurfaces via optofluidic techniques, which can find application in the dynamic generation of colors and tunable optical response for novel display technologies, high-sensitivity refractive index sensors, and anticounterfeiting protection based on chromatic feedback.

## 2. Results

### 2.1. Numerical Simulations

We considered an infinite metasurface composed of Si nanodisks of diameter  $D$  and height  $H$  placed on a semi-infinite glass substrate with a square lattice of period  $P$  and illuminated by a linearly polarized plane wave at normal incidence (**Figure 1a**). The simulated reflectance of the metasurface strongly depends on both the period and the water level  $h_{\text{WL}}$  above the substrate (**Figure 1b**). The spectral boundary between diffractionless and diffractive regions is defined by the substrate RA (also called  $\lambda_s^{\text{RA}}$  or “RA glass”). Here we focus on SLRs that are excited in the diffractionless region ( $\lambda > \lambda_s^{\text{RA}}$ ), which is the region where first-order diffraction into the substrate disappears. We show that the strongest resonant reflectance associated with SLR appears in the diffractionless region in the vicinity of the substrate RA. At the same time, for the wavelengths shorter than the wavelength of the substrate RA, SLRs are absent due to the diffraction scattering into the superstrate and/or substrate.<sup>[39,40]</sup>

Depending on the period of the metasurface, one can distinguish two scenarios for the development of a resonant response, as highlighted by the two horizontal dashed lines in **Figure 1b**, which are separately plotted in **Figure 1c,d**. For longer periods, for example,  $P = 550$  nm (**Figure 1c**), there is no resonance when the metasurface is in air ( $h_{\text{WL}} = 0$ ). The sharp resonance starts emerging only by adding water above a certain threshold level,  $\approx h_{\text{WL}} \geq H = 100$  nm, that is, disks are fully surrounded by water. The quality factor and spectral position of the resonance are indicative of an SLR excitation. For shorter periods, for example,  $P = 450$  nm (**Figure 1d**), the resonance already exists with air as a superstrate and increasing the water level leads to a redshift of the resonance. In both cases, increasing the water level above  $h_{\text{WL}} \geq 400$  nm does not change significantly the shape and position of the resonances, and the superstrate can be assumed as a homogeneous water environment ( $h_{\text{WL}} = \infty$ ). Although a finite water level may introduce Fabry–Pérot resonances,<sup>[29]</sup> they would appear on the left side of the substrate RA and become significant only when the water level is comparable with the wavelength. This is not a regime under investigation in this work. In the next section, based on an analytical model, we explain how these two different regimes of the dynamic response emerge from the SLR excitation and evolve with the refractive index of the superstrate.

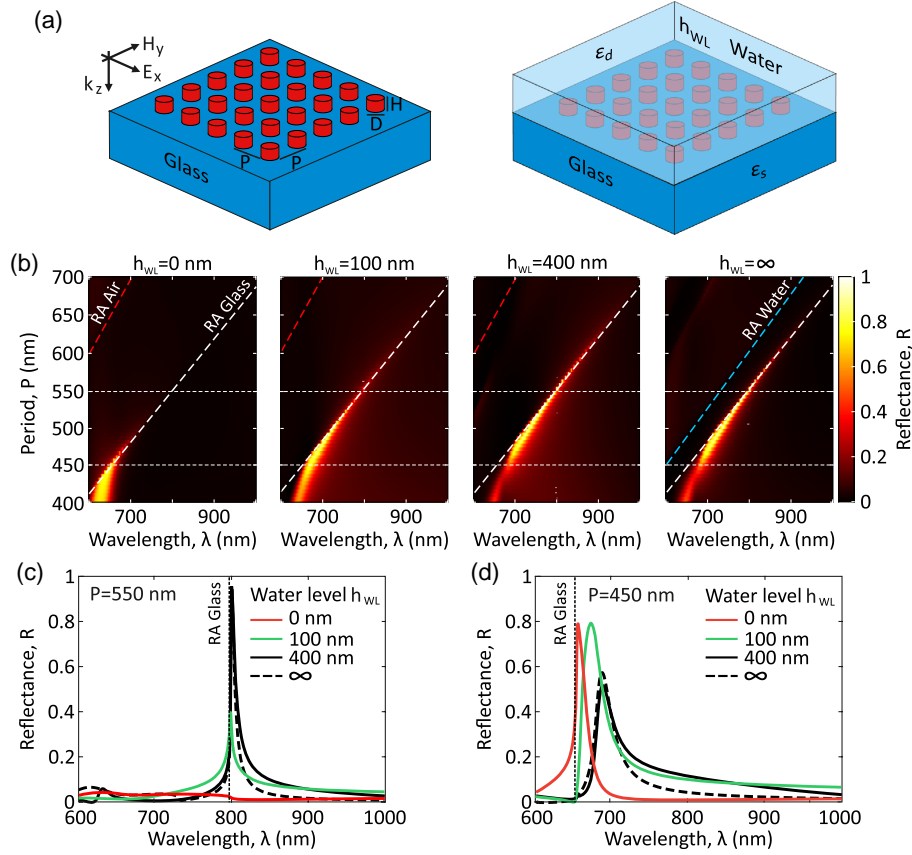


**Figure 1.** Optical properties of a periodic nonlocal metasurface with different superstrates. a) Schematic of a metasurface: Si nanodisks of diameter  $D$  and height  $H$  are arranged in a square array on a glass substrate with periodicity  $P$  along the  $x$  and  $y$  directions. The optical response of the system is controlled by the level of water  $h_{WL}$  on top of a metasurface. The metasurface is illuminated at normal incidence, with  $x$ -linearly polarized light and reflection or transmission is observed. b) Dependence of the reflectance spectra of an infinite array of Si nanodisks with  $D = 200$  nm and  $H = 100$  nm on a period  $P$  for different water levels  $h_{WL}$ . The red (blue) and white dashed lines display the RA conditions for the air (water) superstrate and glass substrate, respectively. c,d) Reflectance spectra of the metasurfaces with (c)  $P = 550$  nm and (d)  $P = 450$  nm, extracted from (b) as indicated with white horizontal dashed lines in (b), illustrating two mechanisms for switching at the limiting values of  $h_{WL}$ : suppression of the resonance in (c) and a spectral shift of the resonance in (d).

## 2.2. Analytical Model

The building block of the metasurface in Figure 1a, that is, a single silicon disk, exhibits mainly electric and magnetic dipole responses in the considered spectral range, regardless of the illumination and surroundings (see the response of a single particle in Section S1 and Figure S1–S5, Supporting Information). Therefore, the coupled-dipole model<sup>[42–44]</sup> can be used for the analytical investigation of the emergence of the metasurface collective resonances observed numerically in Figure 1b. Since the electric dipole coupling dominates over the magnetic one for the metasurface in a homogeneous surrounding (see Section S2, Supporting Information), and the presence of a glass substrate provides only a very weak coupling between electric and magnetic dipoles,<sup>[45]</sup> we will consider only coupling between electric dipoles of the Si disks.

Due to the in-plane translation symmetry and the normal illumination condition (Figure 1a), every particle of an infinite metasurface will have the same electric dipole moment  $p = (p_x, 0, 0)$  defined as<sup>[34,46]</sup>

$$p_x = \frac{\epsilon_0 \epsilon_d \tilde{E}_x}{1/\tilde{\alpha}_{xx}^p - \tilde{S}} \quad (1)$$

where  $\epsilon_0$  and  $\epsilon_d$  are the vacuum permittivity and superstrate relative permittivity, respectively. The tilde symbol is used for quantities defined in the presence of a substrate:  $\tilde{\alpha}_{xx}^p$  is the in-plane electric dipole polarizability of a single disk near a substrate with relative permittivity  $\epsilon_s$  (see Equation S1, Supporting Information),  $\tilde{E}_x$  is the incident electric field at the geometrical disk center (in the absence of the disk), and  $\tilde{S}$  is the dipole lattice sum associated with the electromagnetic interaction (coupling) between dipolar particles of the metasurface on a substrate.

This dipolar system is in resonance when the denominator of Equation (1) vanishes. In the presence of damping associated with material and radiative losses, the conditions for the SLR excitation are

$$\begin{cases} \text{Re}(1/\tilde{\alpha}_{xx}^p) = \text{Re}(\tilde{S}), \\ \min\{|\text{Im}(1/\tilde{\alpha}_{xx}^p - \tilde{S})|\} \end{cases} \quad (2)$$

These conditions include the properties of individual particles via their polarizability and the properties of the array via the dipole lattice sum, which does not depend on the particle properties.<sup>[23]</sup> The conditions in Equation (2) can only be satisfied in the diffractionless region ( $\lambda > \lambda_s^{RA}$ ). A moderate (air/glass or water/glass) dielectric contrast  $\Delta\epsilon = (\epsilon_s - \epsilon_d)$  between the substrate and the superstrate does not significantly affect the broad resonance of  $\tilde{\alpha}_{xx}^p$ , causing only its redshift (Figure S5, Supporting Information). Therefore, the appearance of narrow resonances in the optical response of the metasurface with the changes of the water level (Figure 1b) are related to the effect of  $\Delta\epsilon$  on the lattice sum  $\tilde{S}$  (i.e., on the interparticle interaction).

For a homogeneous glass environment ( $\Delta\epsilon = 0$ ), the lattice sum  $S$  has a divergent singularity at the RA (Figure 2a,b), due to radiative (far-field) coupling between nanoparticles in the array (Figure S6, Supporting Information). Therefore, the resonant conditions in Equation (2) are satisfied and the SLR is excited, as graphically illustrated by the intersection between  $1/\tilde{\alpha}_{xx}^p$  and  $S$  in the diffractionless region in Figure 2a,b (see also Figure S7, Supporting Information, for the case of a homogeneous surrounding).

In the presence of a substrate, the lattice sum  $\tilde{S}$  becomes finite and depends on the dielectric contrast  $\Delta\epsilon$  and the array periodicity. In this case, in addition to  $S$ , the lattice sum also includes a contribution that takes into account the reflection from the substrate  $S^R$ , so that  $\tilde{S} = S + S^R$ .

For both  $S$  and  $\tilde{S}$ , the divergence of the lattice sum only depends on the far-field contribution. The part  $\tilde{S}^{FF}$  corresponding to the far-field interparticle coupling in the metasurface on a substrate can be evaluated as (see Section S3 and Figure S8,S9, Supporting Information)

$$\tilde{S}^{FF} \approx \sum_{l \neq 0}^{\infty} S_l^{FF} (1 + r_l^{(s)}) \quad (3)$$

where  $S_l^{FF}$  is the  $l$ -th far-field lattice term in a homogeneous environment (superstrate) and  $r_l^{(s)}$  is the reflection coefficient for the  $s$ -polarized wave generated by the electric dipole located at a lattice  $l$ -th node and propagating to a node with  $l = 0$  (the distance between these points is  $R_l$ ). The reflection coefficient is then

$$r_l^{(s)} = \frac{1 - \sqrt{R_l^2 / \bar{R}^2 + 1}}{1 + \sqrt{R_l^2 / \bar{R}^2 + 1}} \quad (4)$$

where  $\bar{R} = z_p \sqrt{\epsilon_d / |\Delta\epsilon|}$  is an effective distance determined by the dielectric contrast  $\Delta\epsilon$  with  $z_p$  being the distance from a nanodisk center to the substrate. The value of  $\bar{R}$  can be used to estimate the radius of the long-range (far-field) interaction between nanoparticles in metasurfaces located on a substrate. Importantly, for the metasurfaces considered in Figure 1,  $\bar{R}$  is much smaller than the considered metasurface periods, that is,  $R_l \gg \bar{R}$ . Therefore, from Equation (4), one obtains that

the reflection coefficient  $r_l^{(s)} \simeq -1$  and the far-field sum Equation (3) will be determined by only a finite number of terms due to the suppression of the far-field coupling between the nanoparticles. As a result, the lattice sum in the presence of a substrate does not diverge, having a finite value at the substrate RA.<sup>[40]</sup> However, with an appropriate design, it is possible to satisfy the conditions for the SLR in Equation (2), thus making the proposed approach general and applicable even to metasurfaces with high substrate–superstrate dielectric mismatch.

As shown in Figure 2c,d, the maximum value of the real part of the lattice sum is obtained at the substrate RA ( $\lambda_s^{RA}$ ) and decreases with the increase of the dielectric contrast  $\Delta\epsilon$ . On the one hand, a decreasing lattice sum can lead to  $\text{Re}(\tilde{S}) < \text{Re}(1/\tilde{\alpha}_{xx}^p)$  at the substrate RA, where the conditions in Equation (2) cannot be satisfied, and the SLR is not excited. On the other hand, if the lattice sum is large enough to obtain  $\text{Re}(\tilde{S}) > \text{Re}(1/\tilde{\alpha}_{xx}^p)$  at the substrate RA, then the conditions in Equation (2) are satisfied and the lattice resonance can exist in the diffractionless region. This is due to the fact that  $\text{Re}(\tilde{S})$  monotonically decreases and  $\text{Re}(1/\tilde{\alpha}_{xx}^p)$  monotonically increases with the wavelength in the diffractionless region. Such behavior is observed in Figure 2c, where the condition in Equation (2) is satisfied only for the metasurface with a small dielectric contrast (water/glass) and period  $P = 550$  nm. The second condition in Equation (2) is illustrated in Figure 2e and is satisfied in the diffractionless region for both superstrates. As a result, the reflection spectrum for the water superstrate has a narrow resonant peak with a theoretical quality factor of over 100 (Figure 2g) corresponding to the full circle in Figure 2c. We note that the quality factor of the system can be increased by an order of magnitude (not shown in the figure) by further optimization of the structure (e.g., period and/or superstrate material). Outside of the diffractionless region, the SLR conditions are not fully satisfied; the condition in Equation (2) is fulfilled (Figure 2c) while the condition in Equation (2) is not met due to high losses (Figure 2e).

For the metasurface with a smaller period  $P = 450$  nm, the lattice sum is larger than the inverse polarizability at the substrate RA for both superstrates. As a result, the conditions for the SLRs are satisfied in the diffractionless region for both air/glass and water/glass configurations (Figure 2d,f) and the SLRs are excited with a spectral shift of the resonance depending on the dielectric contrast  $\Delta\epsilon$  (Figure 2h).

For the practical implementation of these two scenarios and their use for the dynamic control of a metasurface response, the following strategy can be followed. Firstly, for a given  $\Delta\epsilon$ , the condition  $\text{Re}(\tilde{S}) > \text{Re}(1/\tilde{\alpha}_{xx}^p)$  must be satisfied at the wavelength of the substrate RA, so the SLR is excited in the diffractionless region. This can be achieved by an appropriate design of the metasurface on the substrate in the presence of an arbitrary superstrate. Then the regime of on/off switching can be realised if an increase of  $\Delta\epsilon$  is sufficient to reach the condition  $\text{Re}(\tilde{S}) < \text{Re}(1/\tilde{\alpha}_{xx}^p)$  at the wavelength of the substrate RA when the SLR is switched off (Figure 2g). In the second scenario, the SLR remains excited but redshifted with a decrease of  $\Delta\epsilon$  (Figure 2h).

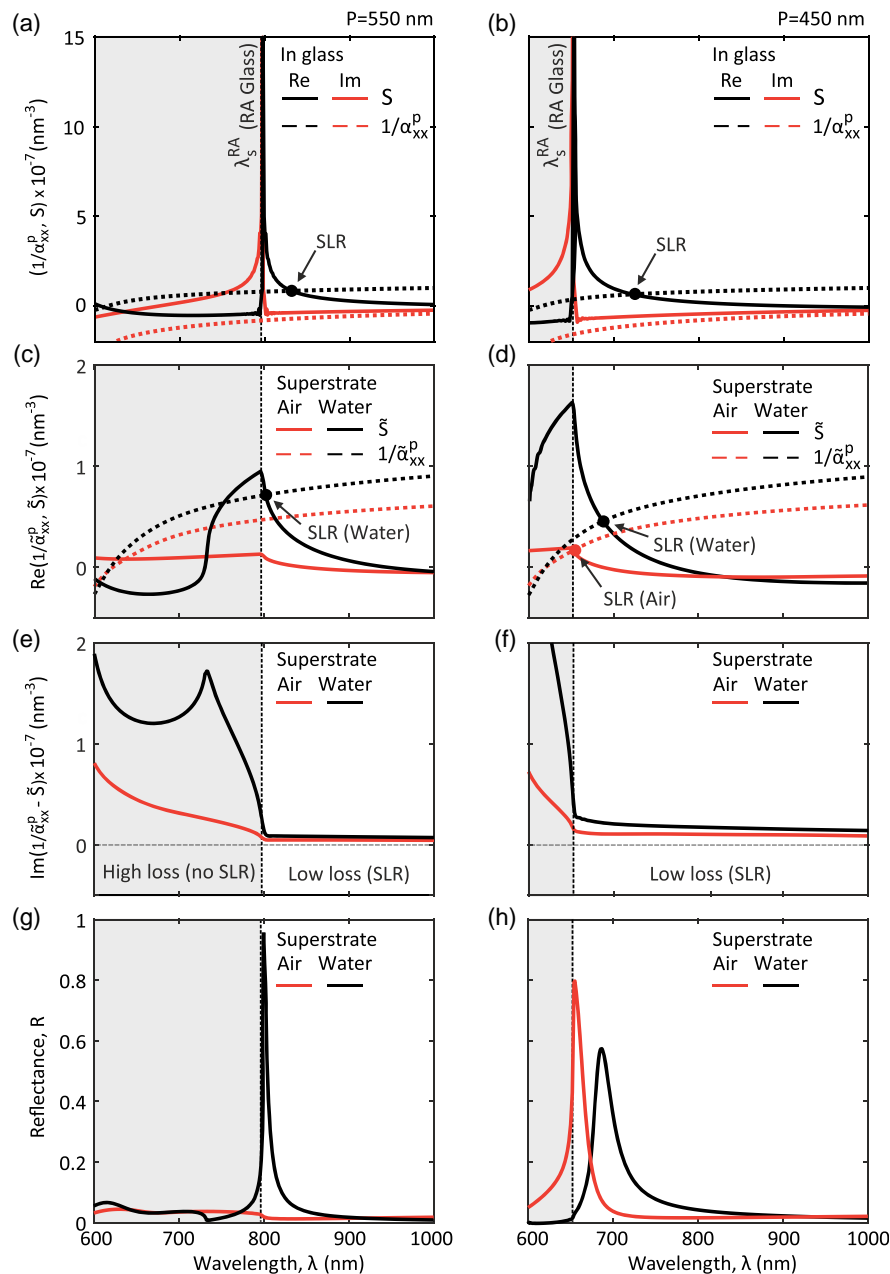


**Figure 2.** Collective lattice resonances. a,b) Spectra of the inverse electric dipole polarizability  $1/\alpha_{xx}^p$  and the full lattice sum  $S$  for a metasurface in a homogeneous glass environment: (black) real and (red) imaginary parts. c,d) Spectra of  $1/\alpha_{xx}^p$  and  $\bar{S}$  for a metasurface on a glass substrate with (red) air or (black) water superstrate (only the real part is shown). e,f) Spectra of the difference of  $1/\alpha_{xx}^p$  and  $\bar{S}$  for a metasurface in the case of (red) air/glass and (black) water/glass superstrate/substrate combinations (only the imaginary part is shown). g,h) Reflectance spectra of a metasurface for (red) air/glass and (black) water/glass cases. (a,c,e,g) correspond to  $P = 550$  nm and (b,d,f,h) correspond to  $P = 450$  nm; in all panels  $D = 200$  nm and  $H = 100$  nm; the superstrate and substrate are considered to be semi-infinite. The vertical black dashed line  $\lambda_s^{RA}$  indicates the position of the RA in the glass substrate. Filled circles in (a,b,c,d) indicate the spectral position of SLRs.

### 3. Experimental Demonstration

#### 3.1. Static Optical Tuneability

To experimentally illustrate the switching and shifting scenarios of SLRs, metasurfaces consisting of  $H = 100$  nm-thick

polycrystalline silicon nanodisks on a glass substrate were fabricated using electron beam lithography (see Section 5 for the details of fabrication and geometrical parameters). Several diameters and periods of the nanodisks (Table 1) were considered in order to investigate tuneability in both switching and shifting scenarios. Transmission and reflection spectra as well as optical

**Table 1.** Geometrical parameters of the fabricated metasurfaces. Nanodisks height is  $H = 100$  nm for all metasurfaces.

Metasurface	$D$ [nm]	$P$ [nm]	Attribute
M1	185	490	Switching
M2	220	440	Shift
M3	225	535	Switching
M4	285	585	Shift

images of the metasurface were recorded to demonstrate the dependence of the optical properties on the refractive index of the superstrate (see Section 5 for the details of the experimental setup).

For the metasurface M1 (Figure 3a), the reflectance spectrum of the metasurface in air does not feature any resonances since lattice resonance is absent due to the large air/glass dielectric contrast (Figure 3c). Immersing the metasurface in water, therefore reducing the dielectric contrast, leads to the switching of the lattice resonance around a wavelength of 730 nm and a strong reflection peak. This demonstrates the principle of switching

an SLR on/off, also corresponding to a change in color (in this case red), which may find application in novel display technologies. Similar switching behavior is observed in transmission (Figure 3e); note that the transmission spectra show also additional resonances due to the absorption of silicon. These spectral features observed in the diffraction region ( $\lambda < \lambda_s^{RA}$ ), along with the tuning of the SLR, determine the color of the metasurface, as we will see in the next section. While absorption in silicon in the visible range prevents us from demonstrating such tuning mechanisms for colors other than red, this can still be achieved using materials with lower absorption, such as silicon nitride<sup>[47]</sup> and diamond.<sup>[48]</sup>

The second type of optical response tuning is demonstrated with a metasurface M2 (Figure 3b), for which the change in surrounding refractive index between air and water leads to a redshift of the lattice resonance from  $\lambda = 680$  nm in air to  $\lambda = 700$  nm in water (Figure 3b,d). The equivalent of Figure 3 with the static optical response tuneability of the metasurfaces M3 and M4 is reported in Figure S11, Supporting Information.

Measured spectra are in overall good agreement with the modeling. Slight deviations in the magnitude and the spectral position of the resonances, which tend to increase as the resonance approaches the substrate RA ( $\lambda_s^{RA}$ ), can be explained by

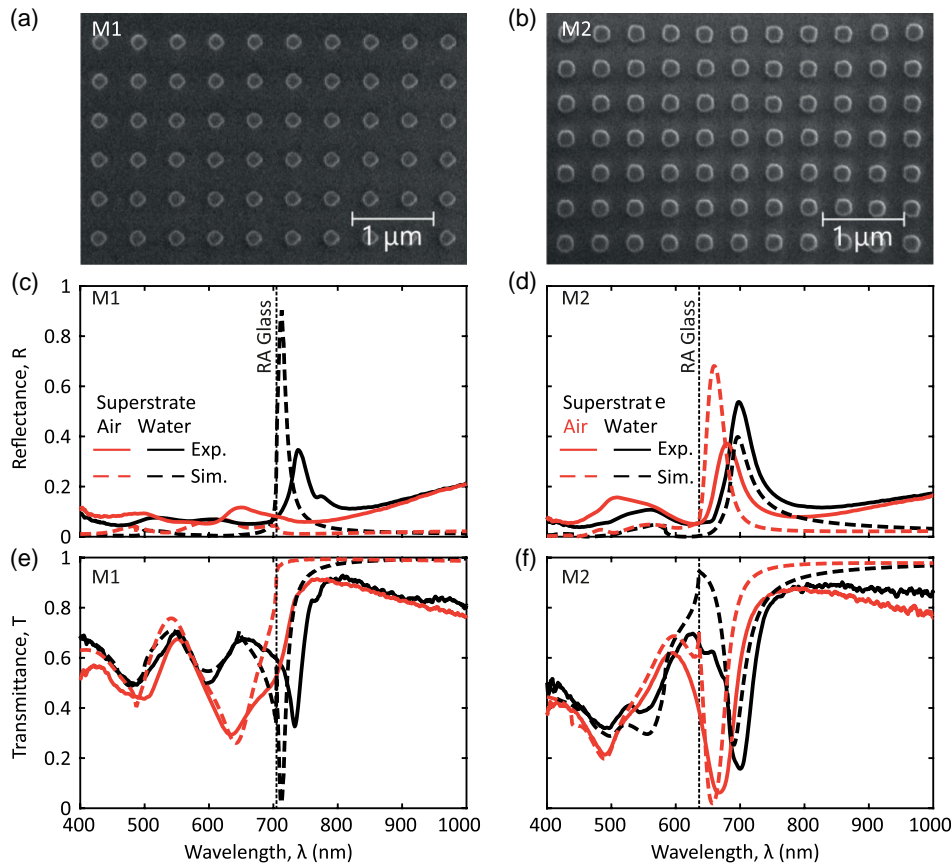


**Figure 3.** Tunable SLRs in nonlocal dielectric metasurfaces. a,b) Scanning electron microscope (SEM) images of the fabricated metasurfaces: (a) M1 with  $D = 185$  nm and  $P = 490$  nm and (b) M2 with  $D = 220$  nm and  $P = 440$  nm. (Oblique view of M1 is shown in Figure S10, Supporting Information). c,d) Reflectance and e,f) transmittance of metasurfaces (c,e) M1 and (d,f) M2 for (red) air and (black) water superstrates: (solid lines) experiment, (dashed lines) simulations. The vertical dashed lines correspond to the spectral position of the RA of a glass substrate  $\lambda_s^{RA}$ .

the finite size of the metasurfaces studied in the experiments (see Figure S12 and S13, Supporting Information for the finite size effects in metasurfaces M1 and M2, respectively).

### 3.2. Dynamic Optical Tuneability

The sensitivity of the optical response associated with the SLR to the thickness of the water layer on top of the metasurface can be used to achieve dynamic tuneability and real-time control of optical spectra and associated coloring of nonlocal dielectric metasurfaces. To demonstrate this, the evaporation of a water droplet deposited on top of the metasurface was monitored by recording the evolution of the transmittance and reflectance spectra every 100 ms until the droplet completely evaporated (Figure 4a,b,e,f). These experiments were conducted for the same metasurfaces

described in the previous section, showing a gradual change in the spectral shape for both reflectance and transmittance. In particular, the time evolution of the reflectance spectra shows a gradual disappearance (metasurface M1, Figure 4a) and shift (metasurface M2, Figure 4b) of the SLR as a function of time and related changes of the apparent colors. Simulated spectra for decreasing water levels (Figure 4c,d,g,h) show a general good agreement with the dynamic evolution of the experimental spectra recorded as a function of time (Figure 4a,b,e,f), with the same discrepancies due to the finite size of the metasurface already discussed in the previous section.

The different trends observed for the reflectance spectra in Figure 4b,d can be understood from Figure S13a,b, Supporting Information, where an increasing discrepancy of the reflectance is observed for the finite and infinite (periodic) size metasurfaces as the SLR gets closer to the substrate RA.

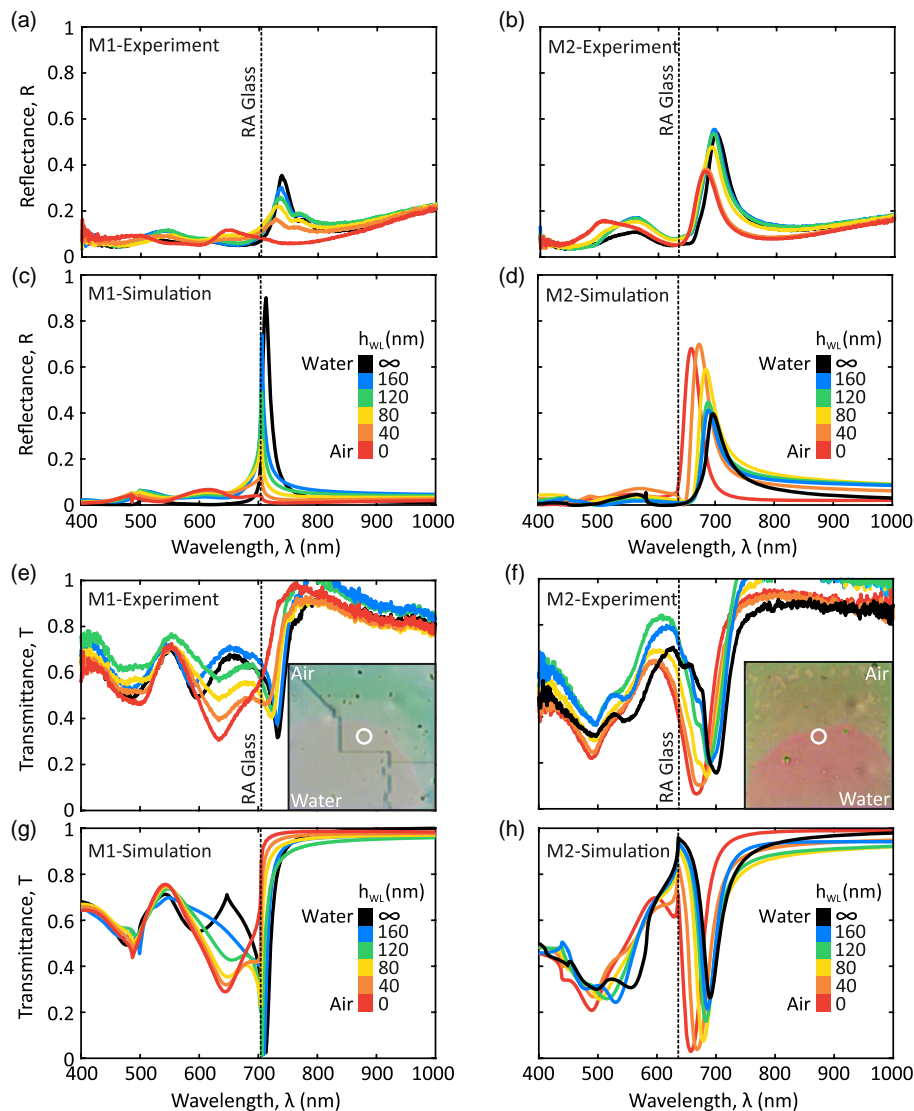


**Figure 4.** Dynamic tuning of nonlocal dielectric metasurfaces. a–d) Reflectance and e–h) transmittance of metasurfaces (a,c,e,g) M1 and (b,d,f,h) M2 while dynamically changing the superstrate between water and air: (a,b,e,f) experimental spectra measured every 100 ms, (c,d,g,f) simulated spectra for different levels of water. The insets in (e,f) show a particular frame of the recorded evaporation process of a water droplet from Supporting Movies M1T, and M2T. The white circles in the frames indicate the collection area of transmitted light in the experiment.

This is due to increasing absorbance (Figure S13g,h, Supporting Information), and thus extinction, for the wavelengths approaching the substrate RA due to scattering losses associated with the metasurface finite size and fabrication imperfections. In general, we notice a better agreement between simulated and experimental spectra in transmission than in reflection. In fact, reflection is inherently related to extinction, which depends on several experimental conditions, such as material absorption (primarily in the diffraction region  $\lambda < \lambda_s^{RA}$ ), scattering losses due to imperfections in the array and metasurface's finite size, lateral radiation (that does not reach the far-field) due to the surface lattice modes, and measurement losses since in the experimental measurements the collection angle is  $< 180^\circ$ . The equivalent of Figure 4 for the dynamic tuneability of the metasurfaces M3 and M4 is reported in Figure S14, Supporting Information.

Snapshots of the metasurfaces during the evaporation of water reveal that the evaporation process occurs by forming a clear and curved front between air and water regions, showing a difference in color (see Supporting Movies) for real-time dynamic color modification upon water evaporation. It is worth mentioning that in our experimental conditions (ambient temperature), water-to-air transition takes place over a few seconds (Supporting Movies and Figure S15a,b, Supporting Information). The process can be accelerated by controlling the temperature of the metasurface. The reflectance and transmittance simulations for water levels between 0 and 400 nm (Figure S15c,d, Supporting Information) show that changes in the reflectance and transmittance spectral features are very sensitive to the water level. These experiments, therefore, demonstrate the possibility of inferring water levels down to the nanometre scale based on the simulated optical response of the metasurface. This could also translate to sensors with high sensitivity for the detection of extremely small amounts of materials on top of the metasurface.

Although the precise control of the water level was not investigated here, these results confirm that such control can provide dynamic tuning of metasurfaces' nonlocal optical response. We remark that our approach only provides a demonstration of the tuneability principle, and more advanced techniques to control the superstrate liquid environment can be used in practical applications, based for example on microfluidic channels<sup>[12]</sup> or the electrowetting effect.<sup>[41]</sup> An example of a microfluidic control scheme is provided (Figure S16, Supporting Information), where pixels (i.e., metasurfaces) are arranged in a matrix form and can be addressed by row, column, or individually, by properly controlling the valves of the microfluidic setup.

## 4. Conclusions

We have proposed and demonstrated a practical and general strategy to dynamically control the nonlocal optical response of an all-dielectric metasurface in reflection and transmission based on the tuning of collective lattice resonances. The approach exploits the dependence of the SLR on the dielectric contrast between substrate and superstrate, which can be achieved by varying the water environment on top of a metasurface, as demonstrated experimentally in this work, or any other tuning mechanism that is capable of modifying the refractive index of a superstrate.

In general, the SLR exists at the wavelength where the equality between the lattice sum and the inverse of the single particle polarizability is satisfied. In a homogeneous medium, the divergence of the lattice sum guarantees that this condition can always be satisfied. However, when the metasurface is located on a substrate, the lattice sum is finite and decreases with increasing the substrate–superstrate dielectric contrast due to the suppression of long-range contributions to the lattice sum. This effectively decreases the number of nanoparticles participating in the collective resonance formation as the dielectric contrast increases, which opens up additional possibilities for the realization and control of SLRs in finite size metasurfaces. We have shown that despite the finite lattice sum, the metasurface can be designed so that the SLR condition is achieved, even for large-index contrast, such as glass–air.

The variation of the refractive index of a superstrate may lead to two scenarios. In the first case, the SLR exists only for higher refractive indexes of a superstrate (low dielectric contrast between a substrate and a superstrate) and is switched off when the dielectric contrast increases. In the second case, the SLR exists in a whole range of the refractive indexes of a superstrate, and the variation of the dielectric contrast results in a spectral shift of the SLR. The experimental demonstration not only reveals changes in the optical response, such as the color tuning, induced by the dynamic variation of the superstrate but also indicates the possibility of measuring water levels down to the nanometer scale by monitoring the optical response of the metasurface.

As demonstrated theoretically and experimentally, the SLR can be achieved despite the finite size of the metasurface. This may be beneficial for the development of pixels in high-resolution displays and optical sensors based on the demonstrated effect. Nonlocal dielectric metasurfaces based on the tuning principles presented here exhibit designed spectral selectivity and dynamic control of spectral response which may find application in color displays, sensors, wavelength-selective tuneable filters and mirrors, augmented reality, anticounterfeiting technology, nonlinear light sources, and in general applications where narrowband tuneability in reflection is required.

## 5. Methods

**Analytical Methods:** The behaviors of single-particle resonances and individual multipole contributions for different excitation and environment conditions are discussed in Section S1, Supporting Information. A comprehensive theoretical description of the response of a metasurface in a homogeneous surrounding environment within the coupled-dipole method is presented in Section S2, Supporting Information. Section S3, Supporting Information, contains the detailed derivation of Equation (3), that is, the lattice sum in presence of substrate in the far-field approximation.

**Numerical Simulations:** The refractive indexes of air, water, and glass used in the simulations were  $n = 1$ ,  $n = 1.33$ , and  $n = 1.45$ , respectively. The refractive index of Si can be found in Figure S1, Supporting Information. Individual multipole contributions (multipole decomposition) of the single-particle resonances were calculated in Ansys Lumerical using the expressions for the multipole moments presented in ref. [49]. The scattering efficiency of a single particle, as well as the reflectance and transmittance of the array, were obtained numerically using full-wave finite-difference time-domain (FDTD) simulations in Ansys Lumerical. For the single particle, a perfectly matched layer (PML) boundary condition was used for all boundaries. In the case of the array, periodic



boundary conditions were used along the in-plane  $x$ - and  $y$ -directions. The fraction of reflectance and transmittance to each grating order was calculated using the “grating order transmission” analysis group object of Ansys Lumerical. Since in the experimental measurements the collection angle was  $< 180^\circ$ , the fraction of reflectance or transmittance within this collection angle was also considered in simulations. Transmittance, reflectance, and absorbance of the finite size metasurfaces (Figure S12 and S13, Supporting Information) were simulated using the “transmission box” analysis group object of Ansys Lumerical. The total-field scattered field (TFSF) source width and the metasurface width differed by a unit cell period  $P$ . The size of the TFSF box in the propagation direction was  $1 \mu\text{m}$ . These settings minimized the influence of the TFSF source size on simulation results. The full dipole sum  $\vec{S}$  in the presence of a substrate was numerically calculated as follows. First, we placed an  $x$ -polarized dipole point source (with a default dipole moment  $p_x$  set by the software, Ansys Lumerical) at  $r_0 = (0, 0, z_p)$  and applied periodic boundary conditions along the in-plane  $x$  and  $y$ -directions with a periodicity  $P$  (i.e., symmetrically respect to  $r_0$  at  $x = y = \pm P/2$ ) and PML boundary condition in the  $z$ -direction. We then calculated the  $x$ -component of the total electric field  $E_x^M$  at  $r_0$ . To exclude the central dipole ( $l=0$ ) contribution, we repeated the above calculation with the PML boundary conditions in all Cartesian directions and subtracted the electric field of the single dipole  $E_x^l$  from the first simulation result  $E_x^M$ . Finally, we calculated the full dipolar sum as  $\vec{S} = \varepsilon_0 \varepsilon_d (E_x^M - E_x^l) / p_x$ .

**Sample Design and Fabrication:** The metasurfaces were fabricated by electron beam lithography on a 100 nm-thick polycrystalline silicon film deposited on a glass substrate. Four different arrays of nanodisks with varying diameters and periods were considered (Table 1). The square array size for each structure was  $100 \mu\text{m} \times 100 \mu\text{m}$ .

**Optical Measurements:** Transmittance and reflectance measurements at normal incidence were performed by illuminating the sample using a tungsten–halogen white light source. The beam, polarized along the  $x$ -axis of the array of nanodisks, was weakly focused onto the sample using a microscope objective with numerical aperture 0.1. In the case of reflectance measurements, the reflected light was collected by the same objective while for transmittance measurements, the transmitted light was collected using a microscope objective with numerical aperture 0.25. The collected light was then coupled to a spectrometer via an optical fiber. The size of the collection area was  $\approx 75 \mu\text{m}^2$ . In both cases, a nonpolarising beamsplitter was used to divert a fraction of the collected light onto a charge-coupled device (CCD) to record images or movies of the sample (Figure S17, Supporting Information). The spectral response of the nanostructures in water was measured by drop casting  $50 \mu\text{L}$  of deionized water onto the nanostructure, fully immersing it. In order to capture the spectral response of the sample while the water level changed between the nanodisks, spectra were recorded every 100 ms until the water droplet fully dried. Movies of the drying process of water on the nanostructures were simultaneously recorded.

## Supporting Information

Supporting Information is available from the Wiley Online Library or from the author.

## Acknowledgements

The authors acknowledge the Deutsche Forschungsgemeinschaft (DFG, German Research Foundation) under Germany's Excellence Strategy within the Cluster of Excellence PhoenixD (EXC 2122, Project ID 390833453), the Alexander von Humboldt Foundation, the ERC iCOMM project (789340), and the UK EPSRC project EP/W017075/1. The authors acknowledge the central computing cluster operated by Leibniz University IT Services (LUIS) at the Leibniz University Hannover. The authors acknowledge the computing time granted by the Resource Allocation Board and provided on the supercomputer

Lise and Emmy at NHR@ZIB and NHR@Göttingen as part of the NHR infrastructure. A.C.L. acknowledges the German Federal Ministry of Education and Research (BMBF) under the Tenure-Track Program. The authors acknowledge Cornerstone for their help in the fabrication of the samples. The publication of this article was funded by the Open Access Publishing Fund of the Leibniz University Hannover.

Open Access funding enabled and organized by Projekt DEAL.

## Conflict of Interest

The authors declare no conflict of interest.

## Author Contributions

I.A., A.B.E., and D.J.R. contributed equally to this work. I.A. performed numerical simulations; A.B.E. performed analytical studies; D.J.R. performed experiments; B.C., A.V.Z., A.B.E. and A.C.L. developed the idea; A.V.Z. and A.C.L. supervised the project. All authors contributed to writing the manuscript.

## Data Availability Statement

The data that support the findings of this study are available from the corresponding author upon reasonable request.

## Keywords

dielectric metasurfaces, dynamic nanophotonics, nonlocal response, optical tuning, surface lattice resonances

Received: September 25, 2023  
Published online: October 20, 2023

- [1] A. M. Shaltout, V. M. Shalae, M. L. Brongersma, *Science* **2019**, 364, eaat3100.
- [2] O. A. M. Abdelraouf, Z. Wang, H. Liu, Z. Dong, Q. Wang, M. Ye, X. R. Wang, Q. J. Wang, H. Liu, *ACS Nano* **2022**, 16, 13339.
- [3] G. Kafaie Shirmanesh, R. Sokhoyan, R. A. Pala, H. A. Atwater, *Nano Lett.* **2018**, 18, 2957.
- [4] J. Sautter, I. Staude, M. Decker, E. Rusak, D. N. Neshev, I. Brener, Y. S. Kivshar, *ACS Nano* **2015**, 9, 4308.
- [5] D. Rocco, A. Zilli, A. Ferraro, A. Borne, V. Vinel, G. Leo, A. Lemaître, C. Zucchetti, M. Celebrano, R. Caputo, C. D. Angelis, M. Finazzi, *New J. Phys.* **2022**, 24, 045002.
- [6] T. Lewi, N. A. Butakov, J. A. Schuller, *Nanophotonics* **2019**, 8, 331.
- [7] T. Zheng, H. Kwon, A. Faraon, *Nano Lett.* **2023**, 23, 5588.
- [8] K. Thyagarajan, R. Sokhoyan, L. Zornberg, H. A. Atwater, *Adv. Mater.* **2017**, 29, 1701044.
- [9] A.-K. U. Michel, S. Meyer, N. Essing, N. Lassaline, C. R. Lightner, S. Bisig, D. J. Norris, D. N. Chigrin, *Adv. Opt. Mater.* **2021**, 9, 2001243.
- [10] S. Abdollahramezani, O. Hemmatyar, M. Taghinejad, H. Taghinejad, A. E. Krasnok, A. A. Eftekhari, C. Teichrieb, S. Deshmukh, M. A. El-Sayed, E. Pop, M. Wuttig, A. Alú, W. Cai, A. Adibi, *Nat. Commun.* **2021**, 13, 1696.
- [11] M. Karimi, M. Z. Alam, J. Upham, O. Reshef, R. W. Boyd, *Nanophotonics* **2023**, 12, 1733.
- [12] Q. Li, J. van de Groep, A. K. White, J.-H. Song, S. A. Longwell, P. M. Fordyce, S. R. Quake, P. G. Kik, M. L. Brongersma, *Nat. Nanotechnol.* **2022**, 17, 1097.

- [13] H. Liu, H. Yang, Y. Li, B. Song, Y. Wang, Z. Liu, L. Peng, H. Lim, J. Yoon, W. Wu, *Adv. Opt. Mater.* **2019**, *7*, 1801639.
- [14] S. Sun, W. Yang, C. Zhang, J. Jing, Y. Gao, X. Yu, Q. Song, S. Xiao, *ACS Nano* **2018**, *12*, 2151.
- [15] H. Li, Y. Xu, X. Zhang, X. Xiao, F. Zhou, Z. Zhang, *Opt. Express* **2022**, *30*, 28954.
- [16] S. Wan, C. Dai, Z. Li, L. Deng, Y. Shi, W. Hu, G. Zheng, S. Zhang, Z. Li, *Adv. Sci.* **2023**, *10*, 2205581.
- [17] K. Shastri, F. Monticone, *Nat. Photonics* **2023**, *17*, 36.
- [18] M. S. Bin-Alam, O. Reshef, Y. Mamchur, M. Z. Alam, G. Carlow, J. Upham, B. T. Sullivan, J.-M. Ménard, M. J. Huttunen, R. W. Boyd, K. Dolgaleva, *Nat. Commun.* **2021**, *12*, 974.
- [19] A. I. Kuznetsov, A. B. Evlyukhin, M. R. Gonçalves, C. Reinhardt, A. Koroleva, M. L. Arnedillo, R. Kiyari, O. Marti, B. N. Chichkov, *ACS Nano* **2011**, *5*, 4843.
- [20] P. Offermans, M. C. Schaafsma, S. R. Rodriguez, Y. Zhang, M. Crego-Calama, S. H. Brongersma, J. Gómez Rivas, *ACS Nano* **2011**, *5*, 5151.
- [21] B. D. Thackray, V. G. Kravets, F. Schedin, G. Auton, P. A. Thomas, A. N. Grigorenko, *ACS Photonics* **2014**, *1*, 1116.
- [22] A. I. Aristov, U. Zywiets, A. B. Evlyukhin, C. Reinhardt, B. N. Chichkov, A. V. Kabashin, *Appl. Phys. Lett.* **2014**, *104*, 071101.
- [23] V. G. Kravets, A. V. Kabashin, W. L. Barnes, A. N. Grigorenko, *Chem. Rev.* **2018**, *118*, 5912.
- [24] S. Zou, N. Janel, G. C. Schatz, *J. Chem. Phys.* **2004**, *120*, 10871.
- [25] V. A. Markel, *J. Phys. B* **2005**, *38*, L115.
- [26] B. Auguié, W. L. Barnes, *Phys. Rev. Lett.* **2008**, *101*, 143902.
- [27] V. Giannini, G. Vecchi, J. G. Rivas, *Phys. Rev. Lett.* **2010**, *105*, 266801.
- [28] A. B. Evlyukhin, C. Reinhardt, U. Zywiets, B. N. Chichkov, *Phys. Rev. B* **2012**, *85*, 245411.
- [29] O. Reshef, M. Saad-Bin-Alam, M. J. Huttunen, G. Carlow, B. T. Sullivan, J.-M. Ménard, K. Dolgaleva, R. W. Boyd, *Nano Lett.* **2019**, *19*, 6429.
- [30] T.-L. Lim, Y. Vaddi, M. S. Bin-Alam, L. Cheng, R. Alaei, J. Upham, M. J. Huttunen, K. Dolgaleva, O. Reshef, R. W. Boyd, *ACS Nano* **2022**, *16*, 5696.
- [31] J. Kelavuori, V. Vanyukov, T. Stolt, P. Karvinen, H. Rekola, T. K. Hakala, M. J. Huttunen, *Nano Lett.* **2022**, *22*, 3879.
- [32] M. Sharma, L. Michaeli, D. B. Haim, T. Ellenbogen, *ACS Photonics* **2022**, *9*, 2702.
- [33] M. Sharma, M. Tal, C. McDonnell, T. Ellenbogen, *Sci. Adv.* **2023**, *9*, eadh2353.
- [34] A. B. Evlyukhin, C. Reinhardt, A. Seidel, B. S. Luk'yanchuk, B. N. Chichkov, *Phys. Rev. B* **2010**, *82*, 045404.
- [35] G. W. Castellanos, P. Bai, J. Gómez Rivas, *J. Appl. Phys.* **2019**, *125*, 213105.
- [36] G. W. Castellanos, S. Murai, T. Raziman, S. Wang, M. Ramezani, A. G. Curto, J. Gómez Rivas, *ACS Photonics* **2020**, *7*, 1226.
- [37] S. Murai, G. W. Castellanos, T. V. Raziman, A. G. Curto, J. G. Rivas, *Adv. Opt. Mater.* **2020**, *8*, 1902024.
- [38] V. E. Babicheva, A. B. Evlyukhin, *J. Appl. Phys.* **2021**, *129*, 040902.
- [39] N. Mahi, G. Lévêque, O. Saison, J. Marae-Djouda, R. Caputo, A. Gontier, T. Maurer, P.-M. Adam, B. Bouhafs, A. Akjouj, *J. Phys. Chem. C* **2017**, *121*, 2388.
- [40] B. Auguié, X. M. Bendana, W. L. Barnes, F. J. G. de Abajo, *Phys. Rev. B* **2010**, *82*, 155447.
- [41] J. Wu, Y. Du, J. Xia, W. Lei, T. Zhang, B. Wang, *Opt. Express* **2019**, *27*, 2521.
- [42] G. W. Mulholland, C. F. Bohren, K. A. Fuller, *Langmuir* **1994**, *10*, 2533.
- [43] O. Merchiers, F. Moreno, F. González, J. Saiz, *Phys. Rev. A* **2007**, *76*, 043834.
- [44] X. Bendaña, F. G. De Abajo, *Opt. Express* **2009**, *17*, 18826.
- [45] A. E. Miroshnichenko, A. B. Evlyukhin, Y. S. Kivshar, B. N. Chichkov, *ACS Photonics* **2015**, *2*, 1423.
- [46] F. G. De Abajo, *Rev. Mod. Phys.* **2007**, *79*, 1267.
- [47] K. Luke, Y. Okawachi, M. R. E. Lamont, A. L. Gaeta, M. Lipson, *Opt. Lett.* **2015**, *40*, 4823.
- [48] A. Taylor, P. Ashcheulov, P. Hubík, Z. Weiss, L. Klimša, J. Kopeček, J. Hrabovský, M. Veis, J. Lorinčík, I. Elantýev, V. Mortet, *Diamond Relat. Mater.* **2023**, *135*, 109837.
- [49] A. B. Evlyukhin, B. N. Chichkov, *Phys. Rev. B* **2019**, *100*, 125415.